JOURNAL OF APPLIED PHYSICS VOLUME 38, NUMBER 13 DECEMBER 1967

Attenuation of Shock Waves in Aluminum*

J. O. Erkman† and A. B. Christensen‡
Poulter Laboratory, Stanford Research Institute, Menlo Park, California

(Received 30 March 1967; in final form 19 July 1967)

Targets of 2024-T351 aluminum were shocked to approximately 110 kbar and 340 kbar by flyer plates having velocities of 0.12 and 0.32 cm/μsec, respectively. Free-surface velocities were determined as a function of target thickness by recording the time of flight across known distances of thin shims which were originally in intimate contact with the surfaces of the samples. The experimental data are believed to be more accurate than any obtained previously. In earlier work it appeared that the free-surface velocity decreased in a stepwise manner as the target thickness was increased. The new data do not show a stepwise decrease, so the simple elastoplastic relations cannot be used to predict attenuation. Some improvement in the predictions was obtained by using a variable shear modulus. The relation between the shear modulus and the strain was obtained from the results of the attenuation experiments. Further improvement may be obtained by the inclusion of the Bauschinger effect in the calculations. Some data were obtained for annealed 1060 aluminum at 110 kbar. The response of 1060 aluminum appears to differ significantly from that of the hard aluminum.

I. INTRODUCTION

The work reported here is an extension of earlier work in which the decay of shock waves in several solids was observed and compared with predictions based on various assumptions concerning the pressure-release curves.[1–3] This earlier work showed the rigidity is significant in several materials studied at pressures up to at least 100 kbar. Agreement between experiment and theory was improved in most cases by assuming an elastoplastic model (in place of a hydrodynamic model) and a particular functional dependence of the yield stress and the shear modulus on the pressure.

Recent studies on aluminum were aimed toward obtaining more explicit information on the variation of the shear modulus and the yield stress at high pressures, and toward obtaining more accurate knowledge of the shape of the pressure-release curve in the immediate vicinity of the shocked state. In this region the elastic and plastic relief waves are most distinctly separated so that the shear modulus and yield stress might be determined. The major portion of the work was performed with 2024-T351 aluminum in the as-received condition. Some work was also performed on type 1060 aluminum to determine whether the high-pressure behavior depends significantly on the initial condition.

Shock waves were produced in specimens of the test materials by impacting them with aluminum plates that had been accelerated to a high velocity by charges of high explosive. The velocities of the plates were determined either optically by means of a streak camera, or electronically by the use of contact pins.

II. EXPERIMENTAL TECHNIQUES

A. Shim Technique for Free-Surface Velocity Measurements

The free-surface velocity of a shock-loaded sample can be determined by several different methods.[4] One of the simplest is to record the time of flight of the free surface across a gap. This method has the disadvantage that it gives an average velocity in those cases in which the shock is not a uniform shock, i.e., the pressure profile is not flat-topped. What is wanted from the measurement is the velocity of the surface at the instant of reflection of the shock wave. The measurement can be made more accurately if a thin (with respect to the stress gradient behind the shock front) shim is held in contact with the specimen. Because the shim is made of the same material as the specimen, it acquires the same velocity as the free surface. If there is any attenuation of the shock, the surface of the specimen is decelerated but the shim continues at uniform velocity. The reflectivity of an aluminum shim changes sufficiently when it is accelerated by a shock so that its initial motion can be detected on a streak camera record (see line *A-A* in Fig. 1). The gap is defined by a glass witness plate (which may be partially coated with gold) set at a known distance from the original position of the shim. When the shim collides with the witness plate, another change of reflectivity occurs, so the arrival can be observed in the record (line *B-B* in Fig. 1). The elastic precursor wave in as-received 2024-T351 aluminum does not change the reflectivity of the shim sufficiently for the precursor to be observed. The gap closure caused by the

* This work was suponsored in whole by the Air Force Weapons Laboratory, Kirtland Air Force Base, New Mexico, under contract No. AF 29(601)-6734.

† Present address: U.S. Naval Ordnance Laboratory, Silver Spring, Maryland.

‡ Present address: University of Denver, Denver, Colorado.

[1] D. R. Curran, J. Appl. Phys. **34**, 2677–2685 (1963).

[2] J. O. Erkman, "Hydrodynamic Theory and High Pressure Flow in Solids," Stanford Research Institute Project No. PGU-3712, Final Report, Contract No. DA-49-146-X2-095, 15 July 1963.

[3] J. R. Rempel and J. O. Erkman, "Shock Attenuation in Solid and Distended Materials," Stanford Research Institute Project No. GSU-4613, Final Report, Contract No. WLTR 64-119, 31 August, 1965.

[4] G. E. Duvall and G. R. Fowles, in *High Pressure Physics and Chemistry*, R. S. Bradley, Ed. (Academic Press Inc., New York, 1963), Chap. IX.

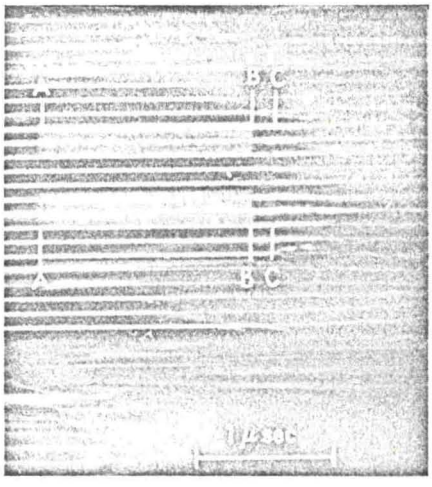

FIG. 1. Typical record of attenuation shot.

unobserved elastic wave causes negligible error in the measurements.[5] When annealed 2024-T351 aluminum specimens, whose thickness was 0.125 in. were hit by a flyer plate of the same material (unannealed) at 110 kbar, the free-surface velocity as recorded by an 0.001-in.-thick shim was essentially the same as the velocity of the projectile plate. In this case the gap was about 0.19 cm, so the shim was in motion for about 1.5 μsec. During this time, relief waves from the back of the projectile plate overtook the front surface of the specimen and slowed it. The record (Fig. 1) shows the arrival of a shim at a witness plate (line *B-B*) and a fraction of a microsecond later the arrival of the surface of the target (line *C-C*). Thus, the time of flight of the shim across the gap gives the initial velocity of the surface even when the shock is not uniform.

B. Fluid Gauge

A second technique was used to obtain a better estimate of the velocity of the relief wave in aluminum. A complete description of the "fluid gauge" has been given elsewhere[6] and only a brief description is included here. The gauge consists of an aluminized Mylar foil (0.00025 to 0.0005 in. thick) suspended in a cell containing a fluid. The bottom of the cell is the specimen in which a shock wave is induced. The foil is oriented at a small angle to the bottom of the cell. When a plane shock wave propagates into the cell, the foil is turned and the amount of turning is monitored by use of the streak camera. Typical records from fluid gauges and the method of reducing the data are given in Ref. 6.

Of present interest is the determination of the depth in water at which the shock is first attenuated. Figure 2 shows the x, t diagram of the interaction of shock waves with surfaces and interfaces after a flyer plate hits the thin specimen of aluminum used as the bottom of a fluid gauge. The shock front ASP is overtaken in the water by the relief wave $BCOP$ at the point P. The wave diagram is constructed in the following way. The slopes of the line segments AB and AS are obtained by using the known flyer-plate velocity to give the particle velocity behind the shocks. Shock velocities are then obtained from the Hugoniot data for aluminum. Interpretation of the gauge record gives both the pressure behind the shock in water and the distance of the point P from the interface. Hugoniot data for water are used to calculate the slope of the line segment SP, which locates point P in the diagram. Both the sound speed and the particle velocity behind the shock are determined by use of the Hugoniot data for water. Hence the line segment OP is drawn. There remains the drawing of the segments BC and CO, a process which is complicated by the refraction due to the wave which was reflected at S. If the thickness of the cell bottom is chosen so that the point P is very close to the interface, the bending of the ray, BCO, introduces an insignificant error in the interpretation of the experiment. For other cases various assumptions can be made concerning the stress–strain relief path for aluminum in order to obtain approximations of the velocity of the relief wave front.

III. EXPERIMENTAL RESULTS

A. Low-Velocity Flyer Plates

Results of experiments in which both the flyer plates and the targets were as-received 2024-T351 aluminum are shown in Table I and in Fig. 3, where the free-surface velocity is plotted as a function of the thickness of the target. Target thicknesses are given in multiples of the flyer-plate thickness, x_0, which for the

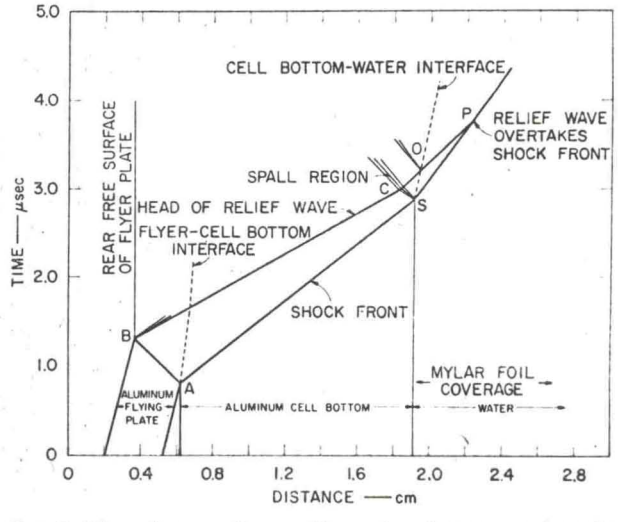

FIG. 2. Time–distance diagram illustrating the wave trajectories in shot 11 762.

[5] At 110 kbar, the elastic precursor separates very slowly from the following plastic wave. Above ~130 kbar, no precursor exists.

[6] T. J. Ahrens and M., H. Ruderman, J. Appl. Phys. **37**, 4758 (1966).

TABLE I. Flying-plate attenuation measurements.

Material	Initial condition	Shot number	Flying plate velocity (cm/μsec)	Flying plate thickness x_0 (cm)	Sample thickness (x/x_0)	Free-surface velocity (cm/μsec)
2024–T351 aluminum	As received	11 484	0.128±0.005	0.315	1.01	0.123±0.002
					5.45	0.118±0.003
					6.06	0.119±0.003
					6.90	0.114±0.002
		11 487	0.128±0.003	0.317	1.00	0.123±0.001
					4.77	0.123±0.001
					6.00	0.116±0.003
					6.83	0.110±0.002
		11 693	0.127±0.002	0.315	4.01	0.125±0.001
					7.05	0.112±0.002
					8.08	0.104±0.001
					9.02	0.099+0.001
		11 694	0.128±0.003	0.317	4.01	0.123±0.001
					7.00	0.106±0.002
					8.00	0.103±0.001
					9.00	0.098±0.003
		11 762	0.130±0.002	0.317	4.06	0.125±0.001
	Annealed	11 414	0.126±0.001	0.317	1.00	0.126±0.001
1060 aluminum	Annealed	11 483	0.127±0.002	0.312	1.02	0.127±0.002
					5.84	0.129±0.002
					6.37	0.122±0.002
					6.99	0.121±0.002
		11 488	0.125±0.003	0.317	4.76	0.127±0.002
					6.31	0.124±0.001
					6.83	0.120±0.001
		11 712	0.129±0.002	0.316	4.02	0.128±0.001
					7.05	0.117±0.001
					8.05	0.118±0.002
					9.05	0.118±0.001
		11 713	0.128±0.002	0.317	4.00	0.126±0.002
					6.99	0.120±0.001
					8.00	0.118±0.001
					8.99	0.115±0.001
2024–T351 aluminum	As received	11 824	0.320±0.005	0.3073	2.07	0.325±0.009
					3.10	0.322±0.003
					4.13	0.327±0.001
					5.16	0.300±0.009
		11 861	0.324±0.005	0.3099	2.04	0.326±0.003
					3.59	0.318±0.009
					7.18	0.281±0.005
					8.19	0.272±0.007

experiments reported here was 0.125 in. (0.317 cm). The estimated errors given in Table I are based on the uncertainty in reading either film records such as that shown in Fig. 1 or records from contact pins.

Shots 11 484 and 11 487 each gave a free-surface velocity of 0.123 cm/μsec for thin targets. In each case the velocity of the flyer plate was 0.128 cm/μsec, so that the free-surface velocity was about 4% less than the velocity of the flyer plate. Lundergan and Herrmann[7] observed that the free-surface velocity was less than the projectile velocity in similar experiments with 6061-T6 aluminum. These results are consistent with elastoplastic theory, the loss in velocity being a counterpart of the phenomenon of residual strain.

When the data are plotted as in Fig. 3 simple elastoplastic theory predicts attenuation to start at a few flyer-plate thicknesses within the target. The drop in free-surface velocity is predicted to be abrupt, the change being that required to reduce the stress by four times the yield.[1] The theory also predicts that the elastic wave from the back of the flyer plate precedes the plastic wave so that there should be a region in Fig. 3 where the free-surface velocity is constant. Such a region is not observed in the data for 2024-T351

[7] C. D. Lundergan and W. Herrmann, J. Appl. Phys. 34, 2046 (1963).

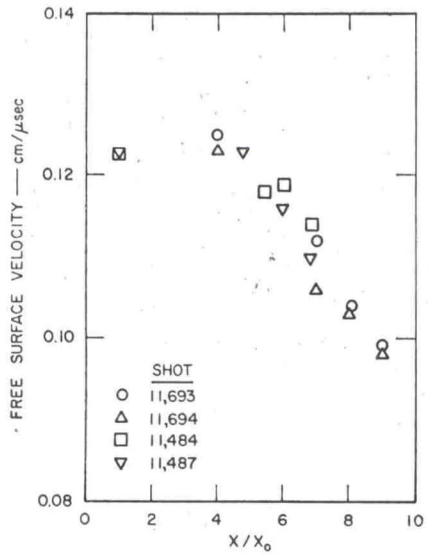

FIG. 3. Free-surface velocity vs shock travel (x/x_0) for 2024-T351 aluminum impacted at 0.125 cm/μsec.

aluminum. If the change in free-surface velocity that is observed is due entirely to an elastic wave, the yield is exceptionally large. It is more likely that there is a Bauschinger effect so that the elastic and plastic waves do not separate, and their combined effects are observed in the experimental results.

Only one experiment was performed with annealed 2024-T351 aluminum. As recorded in Table I, the free-surface velocity of the thin target is the same as the velocity of the flyer plate. This result is consistent with elastoplastic theory if a small yield is used.

Results of attenuation experiments using annealed 1060 aluminum are given in Fig. 4 and in Table I. The average free-surface velocity for thin targets is about 0.127 cm/μsec. This is the same as the average velocity of the flyer plates in the four experiments with 1060 aluminum. Hence this soft aluminum behaves more like a fluid than does 2024-T351 aluminum, for which the free-surface velocity is less than the flyer plate velocity. The data as shown in Fig. 4 also suggest that the elastic relief wave separates from the plastic wave. The evidence for this is the rather abrupt drop in the free-surface velocity starting at about six flyer-plate thicknesses, after which the decrease is slower. More data are needed before an unequivocal conclusion can be drawn. Data should be obtained for targets thicker than nine so that the rate of attenuation due to the plastic wave can be observed.

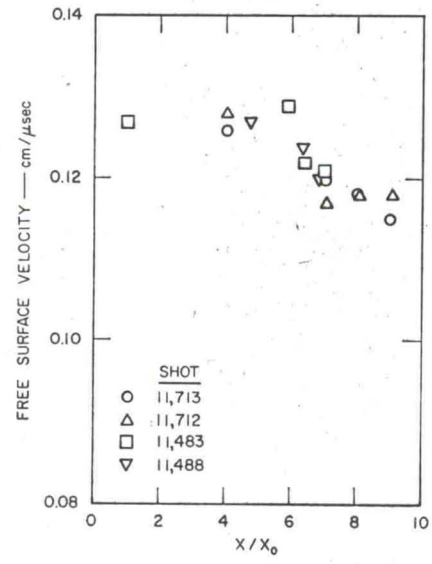

FIG. 4. Free-surface velocity vs shock travel (x/x_0) for 1060 annealed aluminum impacted at 0.125 cm/μsec.

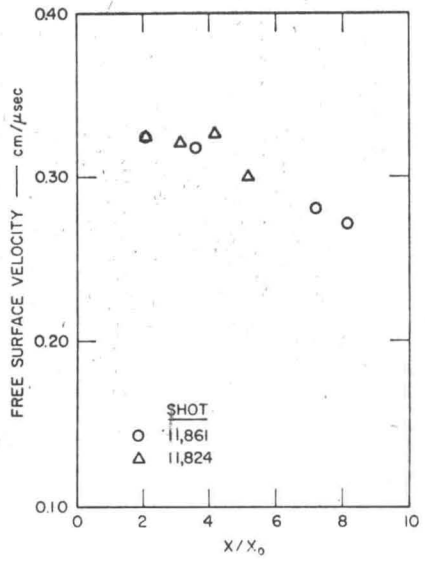

FIG. 5. Free-surface velocity vs shock travel (x/x_0) for 2024-T351 aluminum impacted at 0.32 cm/μsec.

B. 2024-T351 Aluminum (High-Velocity Flyer Plates)

Two experiments were performed with 2024-T351 aluminum in the as-received condition for which the flyer-plate velocity was about 0.32 cm/μsec. This velocity corresponds to a pressure of 345 kbar in aluminum. Results of the shots are given in Fig. 5 and in Table I. The average shim velocity in Shot 11 824 for specimen thicknesses out to 4.1 plate thicknesses is 0.324 cm/μsec. The fact that the free-surface velocity, 0.324 cm/μsec, is slightly greater than the velocity of the flyer plate is one of the interesting results of this experiment. Rigidity must be important because attenuation commences for smaller target thicknesses than predicted by fluid type calculations. The aluminum is heated to a temperature of approximately 500°C so that effects other than those described by simple elastoplastic theory should be expected. One effect appears to be the elimination of the loss of free-surface velocity. If such conjecture is true, experiments at

greater pressure should give free-surface velocities greater than that of the projectile velocities.

Attenuation started between 4.1 and 5.2 plate thicknesses, implying a sound velocity behind the 340-kbar shock of 0.93 cm/μsec. More data are needed for determining if the elastic relief wave and the plastic wave are separated. Because of the results obtained for the lower-pressure experiments, it is doubtful if there is a separation.

IV. CALCULATION OF SHOCK-WAVE ATTENUATION

The attenuation experiments can be simulated by the use of a computer code. Two methods were used to solve the flow equations. One, using the method of characteristics, was restricted to cases in which rigidity was neglected. The equation of state in this code was

$$P=A[(\rho/\rho_0)^\gamma-1], \tag{1}$$

where P is the pressure, ρ is the density, and ρ_0 is the density at zero pressure. When A, γ, and ρ_0 are given the values 0.196 mbar, 4.1, and 2.785 gm/cc, respectively, Eq. (1) satisfactorily represents the Hugoniot data for 24ST aluminum.[8,9]

The other method for solving the flow equations made use of a computer code based on the method developed by von Neumann and Richtmyer in which an artificial viscosity is used to smooth discontinuities in the flow.[10] When material rigidity is neglected, the code uses the equation

$$P=A\mu+B\mu^2+C\mu^2, \tag{2}$$

to represent the equation of state, where P is the pressure in megabars, and $\mu=\rho/\rho_0-1$. In such a case, the Hugoniot and the expansion adiabats are assumed to coincide and are all described by Eq. (2).

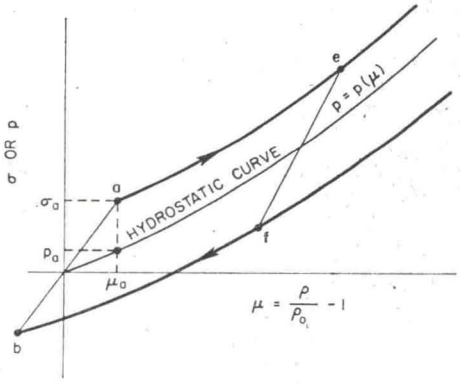

FIG. 6. Schematic diagram of elastoplastic stress–strain relations.

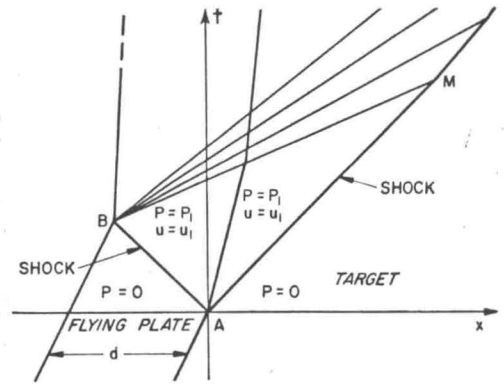

FIG. 7. Physical plane for plate-impact experiment.

A. The Constant Poisson's Ratio Model

An elastoplastic relation is diagrammed in Fig. 6. The hydrostatic curve is represented by Eq. (2), and the upper and lower curves are given by

$$\sigma_x=P\pm 2Y/3, \tag{3}$$

where σ_x is the stress in the direction of propagation of the shock and Y is the yield stress in simple tension, i.e., twice the maximum resolved shear stress. The upper, or loading, curve is made to coincide with the Hugoniot curve just as Eq. (1) was forced to do. Calculated results agreed more closely with experimental results when Y was made to vary with the hydrostatic pressure as

$$Y=Y_0+M(P-P_a), \tag{4}$$

where Y_0 is the initial yield stress, P_a is as defined in Fig. 6, and M is a constant. Values of the various parameters for the elastoplastic equations of state for aluminum are given in Table II. These data are derived from the Hugoniot data given in Ref. 9.

In the derivation of the elastoplastic relations, stress, σ_x, is related to density, ρ, by

$$d\sigma=(K+4G/3)\,d\rho/\rho \tag{5}$$

for an elastic event. In Eq. 5, K is the bulk modulus, G is the rigidity modulus, ρ is the density, and the subscript x has been dropped. In the constant Poisson's ratio model, K is replaced by $-VdP/dV$, where V is the specific volume, P is the hydrostatic pressure, and G is replaced by

$$G=3K\frac{(1-2\nu)}{2(1+\nu)}=\frac{-3V(1-2\nu)}{2(1+\nu)}\frac{dP}{dV} \tag{6}$$

where ν is Poisson's ratio. Combining Eqs. (5) and (6) gives

$$\frac{d\sigma}{d\rho}=c^2=\frac{3(1-\nu)}{(1+\nu)}\frac{dP}{d\rho}, \tag{7}$$

where c is the sound speed and $dP/d\rho$ is the slope of the

[8] S. Katz, D. G. Doran, and D. R. Curran, J. Appl. Phys. **30**, 568 (1959).

[9] M. H. Rice, R. G. McQueen, and M. Walsh, in *Solid State Physics*, F. Seitz and D. Turnbull, Eds. (Academic Press Inc. New York, 1958) Vol. 6.

[10] J. von Neumann and R. D. Richtmyer, J. Appl. Phys. **21**, 232 (1950).

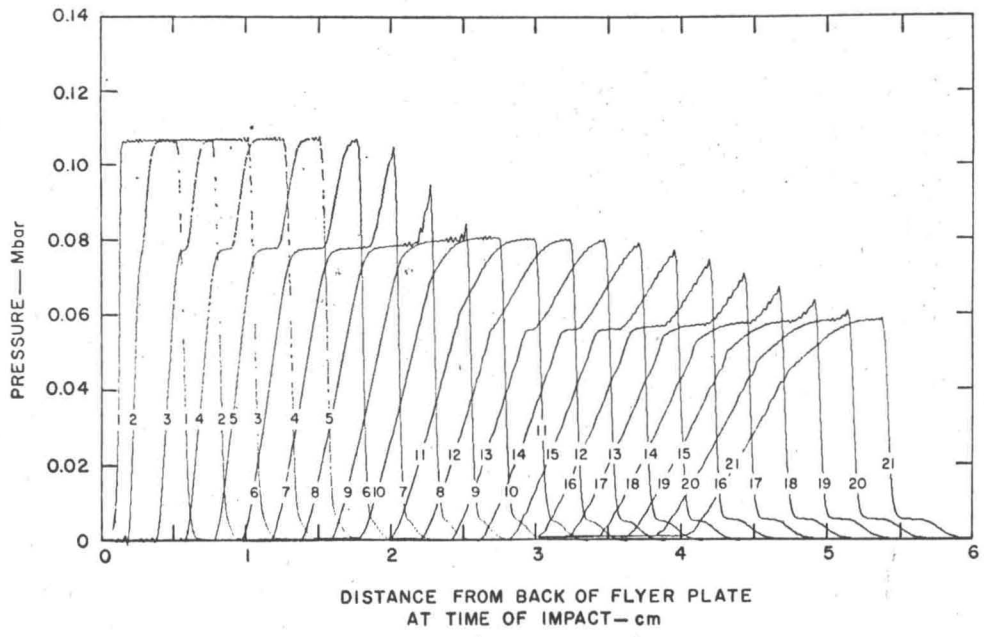

FIG. 8. Profiles of stress for aluminum projectile hitting an aluminum target (projectile thickness 0.322 cm, projectile velocity 0.125 cm/μsec).

hydrostat. Using Eq. (3) then gives

$$c=\left\{\frac{3(1-\nu)}{(1+\nu)}\left[\frac{d\sigma}{d\rho}-\frac{2}{3}\frac{dY}{d\rho}\right]\right\}^{\frac{1}{2}}, \tag{8}$$

so that the elastic sound speed computed from Hugoniot data depends on both ν and Y. This is the speed of sound in the shocked material and is associated with the head of the rarefaction wave BM shown in Fig. 7. The actual velocity of this wave is $u+c$, where u is the particle velocity in the shocked region. For flyer-plate experiments, the particle velocity is determined either by measuring the free-surface velocity of a thin target or by measuring the flyer plate velocity. The latter is more desirable in principle because u is exactly one-half the flyer-plate velocity, while it is only approximately one-half the free-surface velocity.[9] When the particle velocity has been determined, the sound speed is obtained from[11]

$$c=(U-u)[(x+x_0)/(x-x_0)], \tag{9}$$

where x_0 is the thickness of the flyer plate, x is the physical coordinate of the point M in Fig. 7, and U is the velocity of the shock front. Because u is known, U is determined from the Hugoniot relations. Equations (8) and (9) are important links between experimental observations and the theory.

Combining Eqs. (3) and (7) gives

$$\sigma_e-\sigma_f=[(1-\nu)/(1-2\nu)](Y_e+Y_f), \tag{10}$$

where the subscripts refer to the points e and f in Fig. 6 and Y is the yield stress. For $\nu=\frac{1}{3}$, and if Y does not depend strongly on the strain, the usual result,

$$\sigma_e-\sigma_f=4Y, \tag{11}$$

is obtained.

[11] G. R. Fowles, J. Appl. Phys. **31**, 655 (1960).

Some results typical of those obtained with the constant ν model and the Q-code are given in Fig. 8. These results are for the case of an aluminum projectile 0.322 cm thick hitting a semi-infinite target. The pressure vs distance profiles are given at intervals of $\frac{1}{2}$ μsec following projectile impact. The parameters given in column 2 of Table II were used in the elastoplastic stress–strain relations. In Fig. 8, the elastic relief wave reduces the amplitude of the pressure wave by about 30 kbar. Similar profiles of the particle velocity can be obtained from the calculations. Figure 9 shows only the envelope of such particle velocity profiles, along with the results of the characteristic code used with Eq. (1). Comparison of the two sets of results shows the early attenuation which results when the elastoplastic stress–strain relations are used. Experimental results from two previously reported experiments are included in the figure.[3]

B. Arbitrary Shear-Modulus Model

It is not necessary to keep the value of Poisson's ratio constant. If ν is permitted to increase with stress the shear modulus changes with stress in a different way from that used in the earlier calculations [see

TABLE II. Values of parameters for constant ν stress–strain relations for aluminum.

Parameters	Variable-yield model	Constant-yield model	Fluid model
Y (Mbar)	0.0025	0.0025	0.0
M	0.055	0.0	0.0
ρ_0 (g/cc)	2.785	2.785	2.785
A (Mbar)	0.755	0.743	0.765
B (Mbar)	1.29	1.74	1.66
C (Mbar)	1.197	0.329	0.428

TABLE III. Values of experimental parameters for 2024–T351 aluminum.

Parameters	Low-velocity flying plates	High-velocity flying plates
Flyer plate velocity (cm/μsec)	0.125	0.33
Peak stress (Mbar)	0.110	0.345
Sound speed, c (cm/μsec)[a]	0.80±0.02	0.93±0.05
Sound speed, c (cm/μsec)[b]	0.81	...
G (Mbar)	0.54±0.07	0.59±0.25
K (Mbar)	1.27	2.28
$\sigma_e-\sigma_f$ (Mbar)	0.025	0.065
Y_e+Y_f (Mbar)	0.013±0.008	0.025±0.008
Coordinate of point M, Fig. 2	5.5	4.5
Flyer plate thickness (cm)	0.32 (nominal)	0.32 (nominal)

[a] Aluminum free-surface velocity vs depth measurements. [b] Immersed-foil water-gauge measurement.

Eq. (6)]. From Eq. (5) the elastic sound speed is

$$c^2=d\sigma/d\rho=V(K+4G/3)=FV, \qquad (12)$$

where F is called the longitudinal elastic modulus and V is the specific volume. Experiments with flyer plates give values of both c and V, so that F may be calculated. The dependence of F on the stress can be determined if experimental data are available at two or more stress levels. Replacing K with $-VdP/dV$ there results

$$G=3(F-K)/4=3(\rho c^2+VdP/dV)/4. \qquad (13)$$

The quantity dP/dV must first be approximated by $d\sigma_H/dV$ where σ_H is on the upper, or Hugoniot, curve of Fig. 6. Then the variables G, F, and K can be evaluated by using experimentally related values of V and c.

Equation (10) now becomes

$$\sigma_e-\sigma_f=(Y_e+Y_f)(K+\tfrac{4}{3}G)/2G, \qquad (14)$$

or by use of Eq. (12)

$$Y_e+Y_f=1.5[1-(K/\rho c^2)](\sigma_e-\sigma_f), \qquad (15)$$

where K can be approximated as explained above. It was expected that the experiments which give V and c for an elastic wave would also give, at least approximately, values of $(\sigma_e-\sigma_f)$, so that the value of (Y_e+Y_f) could be calculated. Once these values are known as, say, functions of the volume, Eq. (3) can be used to construct a tentative hydrostat, so that another approximation can be made for dP/dV, and the process of calculating G and (Y_e+Y_f) can be repeated. Because the experiments fail to show a definite separation

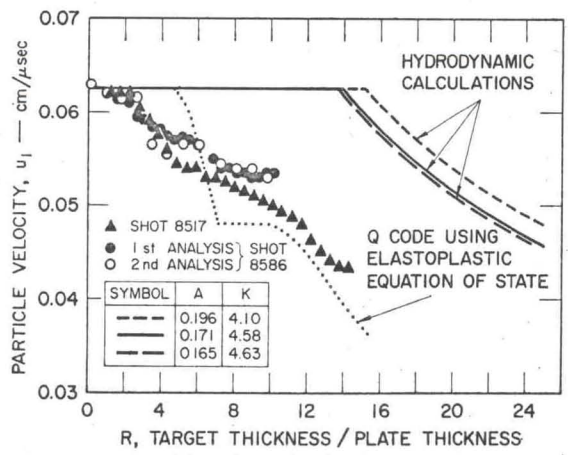

FIG. 9. Peak particle velocity in aluminum target hit by an aluminum projectile.

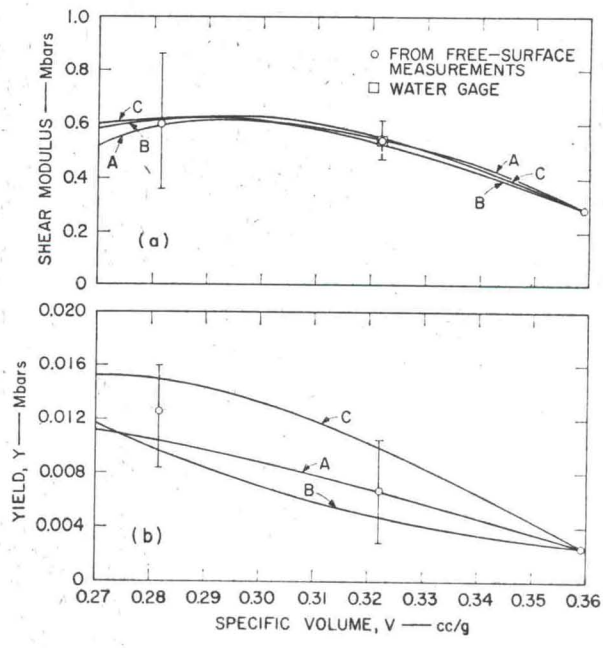

FIG. 10. Shear modulus G and yield stress Y vs specific volume V.

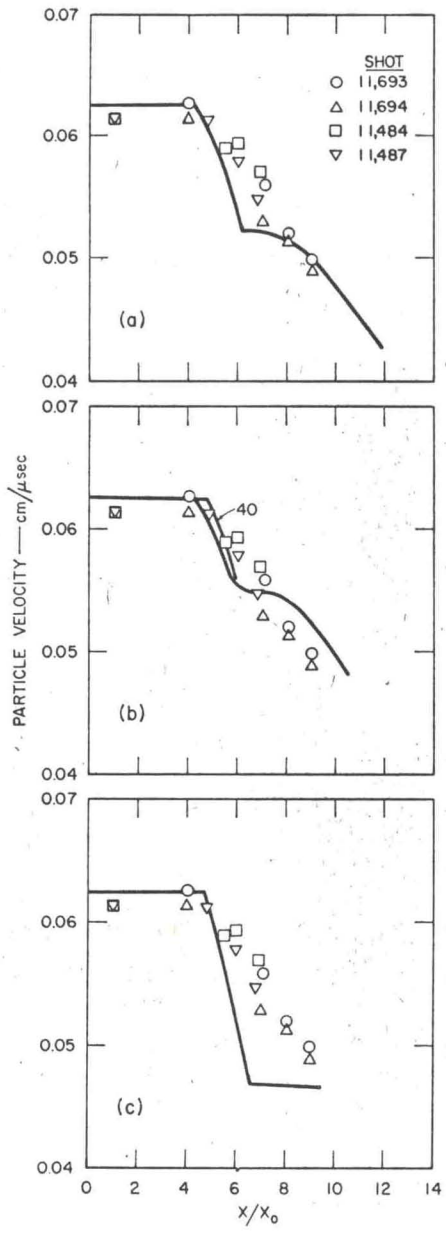

FIG. 11. Comparison of experimental and calculated results for 2024-T351 aluminum impacted at 0.125 cm/μsec.

of the elastic and plastic relief waves, the drop in stress caused by the elastic relief wave is poorly determined. This means that the variation of the yield stress with stress or strain is also poorly determined.

In anticipation of the discussion of the results it can be stated that the shear modulus does not appear to increase indefinitely, a desirable characteristic of this model.

C. Pressure Dependence of Shear Modulus and Yield Stress of 2024-T351 Aluminum

In order to make some comparison of calculated and experimental results it was necessary to assume values of $\sigma_e - \sigma_f$. The value shown in Table III for a 110-kbar shock is the same as that assumed by Curran.[1] The value for the 340-kbar shock was obtained by assuming that all the attenuation observed in Fig. 5 was due to an elastic relief wave, so that the amplitude of the wave is at least 65 kbar.

It should be noted that the uncertainty in the value of the amplitude of the elastic relief wave does not introduce a large uncertainty into the value calculated for the shear modulus. The crucial measurement is the velocity of sound behind the shock front.

Values of G and $(Y_e + Y_f)$ determined from the experiments are shown as functions of the specific volume in Fig. 10. The zero stress value of G, 0.287

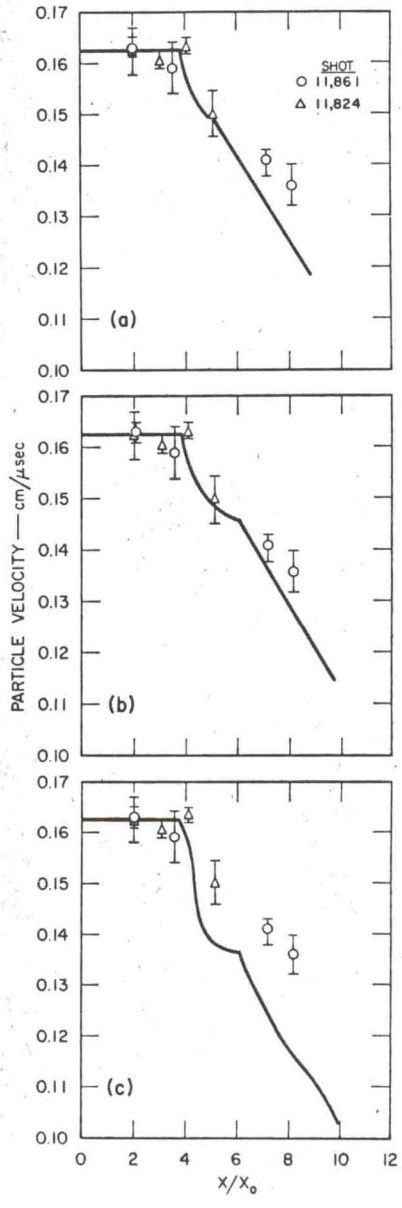

FIG. 12. Comparison of experimental and calculated results for 2024-T351 aluminum impacted at 0.33 cm/μsec.

Mbar,[12] and the approximate value of V_0, 0.0025 Mbar, are also shown in the figure. The possible errors in the data at the high stress point are so large that no conclusive inferences can be drawn about functional relationships. However, relationships can be assumed that are consistent with the data; these permit calculations of shock decay to be made that can be usefully compared with experimental attenuation data. Three such relations are represented by the curves in Fig. 10. These are consistent with the model described in Sec. IV-B in that, for example, if Y varies according to curve A in Fig. 10(b), then G varies as curve A in Fig. 10(a). Curves labeled B and curves labeled C in Fig. 10 are also consistent. The basic difference between the three sets of curves is due to the different ways in which Y is assumed to vary with V. The differences in the curves representing the shear modulus are due to a weak coupling which exists in the mathematical model between Y and G.

The curves shown in Fig. 10 actually represent polynomials in μ, which for the curves labeled A are

$$G=0.287+2.99\mu-6.88\mu^2, \tag{16}$$

and

$$Y=0.0025+0.0407\mu-0.043\mu^2. \tag{17}$$

The hydrostat consistent with the above equations and the Hugoniot for aluminum is represented by

$$P=0.764\mu+1.37\mu^2+1.1\mu^3, \tag{18}$$

where $\mu=(V_0-V)/V$, and the units of G, Y, and P are megabars.

Note that the functions for G exhibit a maximum value near $\mu=0.217$ ($V=0.295$ cc/g). The corresponding pressure is about 250 kbar. It would be of considerable interest to better determine experimentally whether the shear modulus possesses such a maximum along the Hugoniot curve, since this would indicate a trend toward true fluid behavior.

D. Flow Calculations for 2024-T351 Aluminum

Results of flow calculations using the assumptions mentioned above are given in Fig. 11 for the lower-velocity case. The (a), (b), and (c) portions of each figure refer to the fits designated similarly in the preceding section and in Fig. 10.

For lower-impact velocities, fit (a) [Fig. 11(a)] shows reasonable agreement but exhibits a stepwise decrease in particle velocity that is not evident in the data. At higher velocities [Fig. 12(a)] this fit compares favorably at five plate thicknesses but falls off too quickly thereafter.

Fit (b) shows less of a step in the decay curve for lower-velocity impact, but falls off too slowly at the greater target thicknesses [Fig. 11(b)]. The agreement for higher impact velocity is quite good [Fig. 12(b)].

The effect of increasing the number of cells in the calculations is shown by the curve labeled "40" in Fig. 11(b). In this calculation the flyer plate was zoned to contain 40 cells rather than 20 as used in all the other calculations. Zoning the flyer plate with only 20 cells places the apparent point of overtaking at $x/x_0=4.5$; with 40 cells this point moves to $x/x_0=5.0$. Presumably, convergence to the experimentally observed value 5.5 would occur with increasingly fine zoning.

The fit shown as curve C in Fig. 10 clearly gives the least satisfactory fit to the decay curves, as shown in Figs. 11(c) and 12(c).

The results of these attempts to fit the decay curves indicate that the elastoplastic theory as formulated is probably too simple. No step in the decay curves can be clearly identified, at least for 2024-T351 aluminum. This implies that there is no pronounced separation of the elastic and plastic rarefaction waves. The most likely explanation for this difference is that a Bauschinger effect tends to spread the elastic rarefaction so that it merges with the following plastic wave. Bauschinger effects have been observed in plane shock waves at much lower pressures.[13,14]

V. CONCLUSIONS

The data show that the initial attenuation of a shock wave in aluminum is caused by a high-speed rarefaction wave. This wave is assumed to be elastic and its velocity can be accounted for by making reasonable assumptions as to the value of the bulk modulus and the shear modulus. Both moduli are assumed to depend on the strain. Data for 2024-T351 aluminum suggest that the shear modulus may have a maximum value when the stress is between 100 and 340 kbar. Effects of temperature were not accounted for in the behavior of either of the moduli.

In addition, the data suggest that 2024-T351 aluminum exhibits a Bauschinger effect. Annealed 1060 aluminum may not exhibit a strong Bauschinger effect. It appears to behave as a more idealized elastoplastic material than does 2024-T351 aluminum.

ACKNOWLEDGMENTS

The authors wish to thank G. R. Fowles, under whose direction the work was performed, J. H. Hannigan, who assembled the experiment, and D. G. Doran, who critically reviewed both the work and the manuscript.

[12] G. R. Fowles, J. Appl. Phys. **32**, 1475 (1961).

[13] L. M. Barker, C. D. Lundergan, and W. Herrmann, J. Appl. Phys. **35**, 1203 (1964).

[14] O. E. Jones and J. R. Holland, J. Appl. Phys. **35**, 1771 (1964).